Cellular/Molecular

Essential Helix Interactions in the Anion Transporter Domain of Prestin Revealed by Evolutionary Trace Analysis

Lavanya Rajagopalan,[1] Nimish Patel,[2]* Srinivasan Madabushi,[3]* Julie Anne Goddard,[2]* Venkat Anjan,[2] Feng Lin,[4] Cindy Shope,[2] Brenda Farrell,[2] Olivier Lichtarge,[3] Amy L. Davidson,[1] William E. Brownell,[2] and Fred A. Pereira[2,4]

[1]Department of Molecular Virology, [2]Bobby R. Alford Department of Otolaryngology–Head and Neck Surgery, [3]Department of Molecular and Human Genetics, and [4]Huffington Center on Aging and Department of Molecular and Cellular Biology, Baylor College of Medicine, Houston, Texas 77030

Prestin, a member of the SLC26A family of anion transporters, is a polytopic membrane protein found in outer hair cells (OHCs) of the mammalian cochlea. Prestin is an essential component of the membrane-based motor that enhances electromotility of OHCs and contributes to frequency sensitivity and selectivity in mammalian hearing. Mammalian cells expressing prestin display a nonlinear capacitance (NLC), widely accepted as the electrical signature of electromotility. The associated charge movement requires intracellular anions reflecting the membership of prestin in the SLC26A family. We used the computational approach of evolutionary trace analysis to identify candidate functional (trace) residues in prestin for mutational studies. We created a panel of mutations at each trace residue and determined membrane expression and nonlinear capacitance associated with each mutant. We observe that several residue substitutions near the conserved sulfate transporter domain of prestin either greatly reduce or eliminate NLC, and the effect is dependent on the size of the substituted residue. These data suggest that packing of helices and interactions between residues surrounding the "sulfate transporter motif" is essential for normal prestin activity.

Key words: **prestin; OHC; electromotility; nonlinear capacitance; evolutionary trace; auditory**

Introduction

Electromotility is a rapid change in cell shape in response to an applied electrical field. The mammalian outer hair cell (OHC) displays the largest electromotile response of any cell type (Brownell et al., 1985), generating ~50 pN/mV forces at frequencies >50 kHz (Frank et al., 1999). OHCs are specialized mechanosensory cells of the mammalian cochlea that contribute to frequency selectivity of hearing (Brownell et al., 1985, 2001; Snyder et al., 2003; Brownell, 2006). Prestin, a polytopic membrane protein in the OHC lateral wall, is essential for OHC electromotility (Zheng et al., 2000; Dallos and Fakler, 2002; Liberman et al., 2002). When transfected into mammalian cell lines, prestin imparts voltage-dependent capacitance and enhances electromotility in membranes (Zheng et al., 2000; Ludwig et al., 2001; Oliver et al., 2001). This nonlinear capacitance (NLC) is accepted as the signature of electromotility (Santos-Sacchi, 1991; Brownell et al., 2001; Dallos and Fakler, 2002; Snyder et al., 2003; Brownell, 2006).

Received April 17, 2006; revised Oct. 24, 2006; accepted Oct. 25, 2006.

This work was supported by Welch Foundation Grant Q-1391 (A.L.D.), National Institute on Deafness and Other Communication Disorders Grant DC00354 (W.E.B., F.A.P.), National Science Foundation Grant BES-0522862 (F.A.P.), by a postdoctoral training fellowship from the Keck Center for Interdisciplinary Bioscience Training, and National Institute of Diabetes and Digestive and Kidney Diseases Grant R90 DK071504-01 (L.R.). We thank Rodger Brown, Jason Parker, Michael A. Lopez, Gabriela Sanchez, and Haiying Liu for technical assistance.

*N.P., S.M., and J.A.G. contributed equally to this work.

Correspondence should be addressed to Fred A. Pereira, Baylor College of Medicine, 1 Baylor Plaza, Houston, TX 77030. E-mail: fpereira@bcm.edu.

A. L. Davidson's present address: Department of Chemistry, Purdue University, West Lafayette, IN 47907.

DOI:10.1523/JNEUROSCI.2734-06.2006

 0270-6474/06/2612727-08$15.00/0

Cytoplasmic chloride is required for prestin-associated charge movement (Oliver et al., 2001; Fakler and Oliver, 2002; Song et al., 2005), consistent with the membership of prestin in the SLC26A family of sulfate anion transporters (Zheng et al., 2000) that function as anion exchangers (Zheng et al., 2000; Mount and Romero, 2004). The family consists of 11 members (Vincourt et al., 2003) that contain between 11 and 13 putative transmembrane (TM) domains. The second TM contains the highly conserved sulfate anion transporter motif (Markovich, 2001), of unknown physiological significance.

There is minimal secondary and no tertiary structural information for the SLC26A family, and the exact number and topology of transmembrane segments in prestin is debated (Zheng et al., 2000, 2001; Oliver et al., 2001; Deak et al., 2005; Navaratnam et al., 2005). Mutational studies targeting charged amino acids (Oliver et al., 2001), phosphorylation sites (Deak et al., 2005), and glycosylation sites (Matsuda et al., 2004), as well as domain swapping (Zheng et al., 2005) and terminal deletions (Navaratnam et al., 2005; Zheng et al., 2005), have been unable to pinpoint specific domains/residues involved in prestin function. We use evolutionary relationships in protein families to obtain structural and functional information. The computational method of evolutionary trace (ET) ranks individual residues by correlating amino acid variation patterns with functional divergences in protein families (Lichtarge et al., 1996). Clustering of highly ranked residues in the primary, secondary, or tertiary structure can indicate functional sites or molecular recognition surfaces in proteins (Madabushi et al., 2002). ET predictions have proven to be accurate in identifying functional sites in many protein families (Lichtarge et al., 1997; Sowa et al., 2000, 2001; Madabushi et al.,

Table 1. Primers used for prestin mutagenesis

Primer	Sequence
Prestin^{WH1}Fwd	5′TTCAGCTTCCCCAAGGCTTA***TGG***TTC***TGG***ATG***TGG***GCGGCTGTTCC
Prestin^{WH1}Rev	5′TAAGCCTTGGGGAAGCTGAAGCACGCCGGT
Prestin^{WH2}Fwd	5′CTGTTCCTCCGGTGTTCGGC***TGG***TACTCTTCA***TGG***TATCCTGTTAT
Prestin^{WH2}Rev	5′GCCGAACACCGGAGGAACAGCCGCGAGCAT
A100WFwd	5′TTCCCCAAGGCTTA***TGG***TTCGCAATGCTCGC
A100WRev	5′GAGCATTGCGAA***CCA***TAAGCCTTGGGGAAGC
A100VFwd	5′TTCCCCAAGGCTTA***GTG***TTCGCAATGCTCGC
A100VRev	5′GAGCATTGCGAA***CAC***TAAGCCTTGGGGAAGC
A100LFwd	5′TTCCCCAAGGCTTA***CTG***TTCGCAATGCTCGC
A100LRev	5′GAGCATTGCGAA***CAG***TAAGCCTTGGGGAAGC
A100GFwd	5′TCCCCAAGGCTTA***GGA***TTCGCAATGCTCGC
A100GRev	5′GAGCATTGCGAA***TCC***TAAGCCTTGGGGAAGC
A100SFwd	5′TTCCCCAAGGCTTA***TCC***TTCGCAATGCTCGC
A100SRev	5′GCGAGCATTGCGAA***GGA***TAAGCCTTGGGG
A102WFwd	5′CTTAGCCTTC***TGG***ATGCTCGCGGCTGTTCC
A102WRev	5′CAGCCGCGAGCAT***CCA***GAAGGCTAAGCC
A102GFwd	5′CTTAGCCTTC***GGA***ATGCTCGCGGCTGTTC
A102Grev	5′CAGCCGCGAGCAT***TCC***GAAGGCTAAGCC
A102VFwd	5′CTTAGCCTTC***GTG***ATGCTCGCGGCTGTTCC
A102GRev	5′CAGCCGCGAGCAT***CAC***GAAGGCTAAGCC
A102LFwd	5′CTTAGCCTTC***CTG***ATGCTCGCGGCTGTTCC
A102LRev	5′CAGCCGCGAGCAT***CAG***GAAGGCTAAGCC
A102SFwd	5′GCTTAGCCTTC***TCC***ATGCTCGCGGCTGTTC
A102SRev	5′GAACAGCCGCGAGCAT***GGA***GAAGGCTAAGC
L104WFwd	5′CCTTCGCAATG***TGG***GCGGCTGTTCCTC
L104Wrev	5′GAACAGCCGC***CCA***CATTGCGAAGGCTAAGC
L104VFwd	5′CCTTCGCAATG***GTC***GCGGCTGTTCCTC
L104VRev	5′GAGGAACAGCCGC***GAC***CATTGCGAAGG
L104IFwd	5′CCTTCGCAATG***ATC***GCGGCTGTTCCTC
L104Rev	5′GAGGAACAGCCGC***GAT***CATTGCGAAGG
L113WFwd	5′CTCCGGTGTTCGGC***TGG***TACTCTTCATTTTATCCTG
L113Wrev	5′GGATAAAATGAAGAGTA***CCA***GCCGAACACCGGAGG
F117WFwd	5′GTGTTCGGCCTGTACTCTTCA***TGG***TATCCTGTTATCATGTACTG
F117WRev	5′GTACATGATAACAGGATA***CCA***TGAAGAGTACAGGCCGAACAC
A305VFwd	5′GGAACTGGCATTTCC***GTG***GGGTTTAACTTGC
A305VRev	5′GCAAGTTAAACCC***CAC***GGAAATGCCAGTTC

Fwd, Forward; Rev, reverse.

2004). ET analysis of prestin identified clustered trace residues with high rank, which were subjected to systematic mutational and functional studies. Prestin mutants were all expressed at the plasma membrane in human embryonic kidney (HEK 293) cells with equal efficiency as wild type (WT). However, several mutants displayed reduced or no NLC, depending on the type and size of residue substitution. The results suggest that residues in the sulfate anion transporter domain region are essential for normal prestin function.

Materials and Methods

Creation of plasmids. To create the prestin plasmid, we inserted a primer, 5′ACCATGTACCCATACGATGTTCCAGATTACGCTCTC3′, containing the hemagglutinin antigen (MYPYDVPDYAL) in-frame with the ATG start codon of the gerbil prestin cDNA (GenBank accession number AF230376) in pBluescript (Stratagene, La Jolla, CA). The 2.7kb *Bam*HI and *Xho*I fragment containing prestin cDNA was then subcloned into the pIRES–hrGFP-1a vector (phosphorylated internal ribosomal entry site–humanized *Renilla reniformis* green fluorescent protein-1a vector) (Stratagene). These constructs produce green fluorescent protein (GFP) as an independent protein that enables identification of transfected cells. Site-directed mutations were then created in this construct using either the GeneTailor (prestin^{WH1} and prestin^{WH2}; Invitrogen, Carlsbad, CA) or the Quikchange (all other mutants; Stratagene) site-directed mutagenesis system. The primer sequences used are presented in Table 1 (mutated codons are in italics and bold).

The A102G/L113W mutant was created using L113W primers on the A102G mutant template. All constructs were sequenced in their entirety using five overlapping primers and were found to have no mutations other than the ones specifically introduced.

Immunofluorescence: detection of prestin in HEK 293 cell membranes. HEK 293 cells were maintained in DMEM (Mediatech, Herndon, VA) with 10% fetal bovine serum (FBS) (Invitrogen, Carlsbad, CA) and allowed to grow to ~80–100% confluence before passaging. For transfections, 100,000 cells were seeded on coverslips placed in each well of 24-well plates, allowed to grow to ~50% confluency, and transfected with either wild-type or mutant prestin DNA, in a 3:1 ratio with FuGene 6 (Roche, Indianapolis, IN). Transfected cells were cultured for 48 h, rinsed with PCM (PBS with 1 mM $CaCl_2$ and 0.5 mM $MgCl_2$), incubated for 1 h on ice with wheat-germ agglutinin (WGA)–biotin (10 μg/ml), rinsed again with PCM, and fixed with 4% paraformaldehyde (15 min). The cells were then washed twice with PBS (10 min each) and permeabilized with PBS–Triton X-100 (3 min) before blocking with 1% BSA in PBS for 1 h at room temperature (RT). Anti-hemagglutinin (HA) (dilution 1:1000; Cell Signaling Technology, Beverly, MA) primary antibody in 1% BSA was added and incubated for 3 h at RT or overnight at 4°C. The cells were washed again three times in PBS (10 min each) before addition of AlexaFluor-594 and AlexaFluor-350 goat anti-mouse secondary antibody (dilution 1:2000; Invitrogen) and incubated for 1 h at RT. After three PBS washes (10 min each), the coverslips were mounted inverted on glass slides with Fluoromount antifade reagent (Invitrogen) and sealed with nail polish. The HA-tagged prestin proteins were viewed, and deconvolution images were captured on a DeltaVision deconvolution microscope (oil-immersion lens, 63× magnification). Images were analyzed using SoftWoRx image restoration software (Applied Precision, Issaquah, WA).

HEK 293 transfections for electrophysiological measurements. When transfecting cells for electrophysiological studies, HEK 293 cells were seeded at a density of ~100,000 cells per well on a 60 mm plate and incubated overnight. The medium in the wells was then replaced with fresh DMEM plus 10% FBS. For transfection, 250 μl of serum-free DMEM was mixed with 7.5 μl of FuGene6 (Roche), incubated for 5 min at room temperature, followed by addition of plasmid DNA (2 μg) and incubation for an additional 30 min. The mixture was then evenly added to the culture medium in the 60 mm plate containing HEK 293 cells. The plates were maintained in a water-jacketed CO_2 incubator (Nuaire, Plymouth, MN) at 37°C in 5% CO_2 for 12–18 h after addition of the DNA–FuGene complex. The cells were trypsinized for 5 min using 2 ml of 0.25% trypsin–EDTA (Invitrogen) at 37°C. The cells were pelleted (800 × *g*) and resuspended in 1 ml of DMEM plus 10% FBS and seeded onto a poly-D-lysine-coated glass-bottom culture dishes (MatTek, Ashland, MA) containing 3 ml of DMEM plus 10% FBS at a concentration of 20,000–50,000 cells per dish and placed in incubator at 37°C in 5% CO_2 overnight.

Electrophysiological measurements. Electrophysiological data were obtained from cells using the whole-cell voltage-clamp technique. Our recording techniques are fully described previously (Farrell et al., 2006); a brief description follows. Culture dishes containing transfected cells were placed on the stage of an inverted microscope (Zeiss, Gottingen, Germany). The cells were extensively perfused with the extracellular solution containing Ca^{2+} and K^+ channel blockers (in mM: 100 NaCl, 20 CsCl, 20 tetraethylammonium-Cl, 10 HEPES, 2 $CoCl_2$, 1.47 $MgCl_2$, and 2 $CaCl_2$) before recording. Cells were visualized under 63× or 100× magnification oil immersion objectives (Zeiss) with a halogen light source. Single isolated cells displaying robust GFP fluorescence (488 nm) were selected for recordings. All recordings were performed at room temperature (23 ± 1°C). Patch pipettes (quartz glass) with resistances ranging from 1.5 to 4 MΩ were fabricated using a laser-based micropipette puller (P-2000; Sutter Instruments, Novato, CA). The pipettes were filled with an intracellular solution, also containing channel blockers (in mM: 140 CsCl, 2 $MgCl_2$, 10 EGTA, and 10 HEPES). The pH and osmolality of both external and internal solutions were adjusted to 7.2 ± 0.02 and 300 ± 2 mOsm/kg with the addition of CsOH and glucose, respectively.

Cell membrane admittance *Y* was measured with the patch-clamp technique in the whole-cell mode. An electrical seal (>1 GΩ) was formed between the pipette and cell membrane then the pipette capacitance was

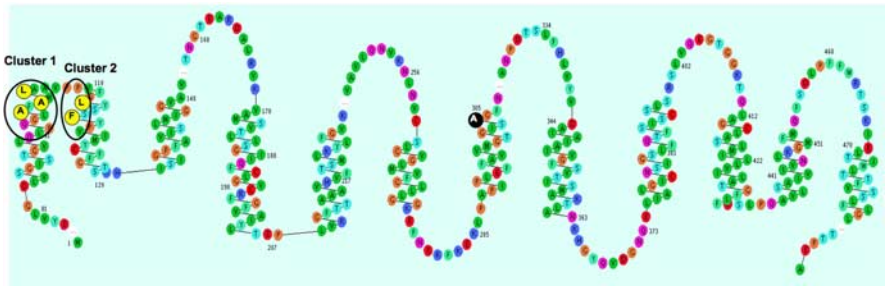

Figure 1. Predicted secondary structure and topology of prestin. Model predicted by ET analysis of the hydrophobicity profile of prestin orthologs. Trace residues examined are highlighted (yellow), and clustered residues are circled. Ala305 is highlighted in black. The schematic was constructed using the ET-predicted helix regions in the web-based service RbDE [residue-based diagram editor (Konvicka et al., 2000)].

corrected with the compensation circuitry of an amplifier (Axon 200B; Molecular Devices, Union City, CA). Once the cell was in the whole-cell mode at 0 mV, the cell admittance was monitored during a direct current (DC) voltage ramp. During a ramp, the voltage increased at 0.3 V/s from −0.16 to 0.16 V. The holding potential was 0 V before and after the ramp. Voltages were measured relative to an Ag/AgCl reference electrode in the extracellular solution. Admittance (Y) was probed with dual-frequency stimulus (Santos-Sacchi et al., 1998). The stimulus was the sum of two 10 mV peak-to-peak sine waves at frequency f of 390.625 Hz and $2f$ of 781.25 Hz. The cell parameters were calculated from the admittance as described previously (Farrell et al., 2006)

The conductance b was also determined experimentally with a DC protocol, in which the voltage was ramped from −0.16 to 0.16 V. Briefly, a square wave pulse with amplitude of 0.01 V was applied to the cell via the pipette. The current was sampled every 10 or 100 μs for 1000 times (400 points before pulse, 500 points during the pulse, and 100 points after the pulse) at each voltage. The conductance b was then calculated from the change in the steady-state part of the measured current relative to the change in the voltage. $C(V)$ was the same (within 100 fF) when it was calculated with $b(V)$ determined experimentally with a DC protocol or with $b(V)$ calculated directly from the equations by use of the admittance measurements.

In all representations, the nonlinear portion of the capacitance was normalized to the difference between linear capacitance and peak capacitance, as indicated in the equation below. Linear capacitance was usually taken as the capacitance at +100 mV, except in the case of A100G, for which linear capacitance was taken as that at −100 mV. Peak capacitance differed with each mutant: $C_{norm} = [C(V) - C_{lin}]/[C(V_{pkc}) - C_{lin}]$, where $C(V)$ is the calculated capacitance at voltage V, $C(V_{pkc})$ is the calculated capacitance at peak voltage V_{pkc}, and C_{lin} is linear capacitance (defined above). Those mutants that did not exhibit bell-shaped capacitance curves were normalized as above, using the $[C(V_{pkc}) - C_{lin}]$ value from WT prestin (0.29). The capacitance curves were fit to a Boltzmann equation as described previously (Oliver and Fakler, 1999), and the charge density was calculated by dividing maximum charge transferred (Q_{max}) by linear capacitance (C_{lin}).

Results

ET defines clusters of trace residues in prestin

ET analysis was performed on 60 prestin homologs to determine which residues may be important for the unique functional properties of prestin (supplemental data, available at www.jneurosci.org as supplemental material). [A comparable ET analysis can be performed using software accessible at our website (http://mammoth.bcm.tmc.edu/server.html).] Prestin, in particular the mammalian prestins, may be unique within the SLC26A family in their ability to confer nonlinear capacitance into cell membranes. Therefore, an analysis of prestin and other SLC26A family members over different phylogenetic branches yields information on evolutionarily important residues. Furthermore, ET looks for positions that are not merely conserved but conserved within each homolog subfamily, at the same level (rank) of phylogenetic divergence. As a result, trace residues can be all at once variable across the diverse members of an entire family yet invariant within each separate individual evolutionary branch and thus strongly linked to the specific function of each of these branches. The rank is the smallest number of subfamilies into which the global superfamily needs to be divided so as to see the residue conserved within each subfamily.

In addition, a model of prestin secondary structure was constructed using the hydrophobicity profile of prestin orthologs in combination with ET analysis. ET ranks of residues within a membrane helix are observed to show a regular periodicity. A suggested topology is supported by ET analysis if it is in agreement with periodicity of evolutionary conservation seen in helices. Helix predictions were done as usual, using hydrophobicity-based calculations (TopPred software, 10 helices; and THMM software, 12–13 helices), and ET analysis confirmed the 12 TM topology in prestin, although the 10 helices predicted by TopPred did not coincide with the periodicity of residue ranks. The model provides an estimate of the lengths of TM helices and connecting loops (Fig. 1). The resultant 12 helixes are as follows: H1, D83 to A105; H2, F111 to S129; H3, I132 to A148; H4, V178 to T206; H5, L209 to V232; H6, S261 to K276; H7, A288 to F307; H8, D342 to N363; H9, L375 to S398; H10, L412 to F432; H11, A438 to M453; H12, E468 to L484. The assignment of the helix limits, positions, and even number of TMs is consistent with the intracellular location for the N and C termini (Ludwig et al., 2001) and the extracellular location of the N-glycosylation (N163 and N166) sites for prestin (Matsuda et al., 2004). In addition, because ET cannot predict directionality of helices, our model is consistent with that of Deak et al. (2005).

Two sets of top-ranked ET residues that are clustered in both the primary and secondary structures were chosen for mutational analysis. These residues ranked high in an ET analysis of mammalian prestin homologs (supplemental Fig. 1*b*, available at www.jneurosci.org as supplemental material) and low in a global SLC26A family ET analysis (supplemental Fig. 1*a*, available at www.jneurosci.org as supplemental material). The first highly conserved cluster consists of three residues (A100, A102, and L104) within the first transmembrane helix (H1, D83 to A105), near the extracellular face (Fig. 1). Previous ET studies on other polytopic membrane proteins suggest that such clusters may be involved in interactions responsible for maintaining the integrity of the membrane domains (Geva et al., 2000). The clustered residues identified in prestin are ranked 1 (A100), 3 (A102), and 1 (L104). A triple mutant containing tryptophan (W) substitutions at all three positions (prestin^{WH1}, A100W, A102W, and L104W) was created to maximize disruptive interactions. We then made a panel of substitutions at each residue, individually substituting A100 and A102 with W, glycine (G), valine (V), leucine (L), and serine (S), and L104 with W, V, and isoleucine (I). A second ET cluster (Fig. 1) comprising residues L113 (rank 1) and F117 (rank 2) in the second transmembrane helix (H2, F111 to S129) was also mutated to W, in combination (prestin^{WH2}) and individually (L113W and F117W).

Wild-type prestin and mutants are expressed in the plasma membrane of HEK 293 cells

To verify plasma membrane expression, immunofluorescence in combination with deconvolution microscopy was used to visualize cellular localization of WT prestin and prestin mutants. Prestin is expressed at the cell membrane by 48 h after transfection (Fig. 2*A*, red fluorescence). Prestin is also present in the endoplasmic reticulum/Golgi trafficking system (Fig. 2*A*), because it is continuously produced by the strong cytomegalovirus promoter for up to 96 h after transfection (data not shown). WT and prestin mutant expression (Fig. 2*A–Q*, red fluorescence) was also colocalized with WGA (Fig. 2*A–Q*, blue fluorescence), which binds GM1 gangliosides on the external cell surface (Monsigny et al., 1980). In most cases, cell surface expression of WT and prestin mutants was indistinguishable at 48 h after transfection (when electrophysiological measures were performed). A possible exception is L104W, which appears to show a reduced level of membrane expression; however, at least a proportion of this mutant is seen at the membrane.

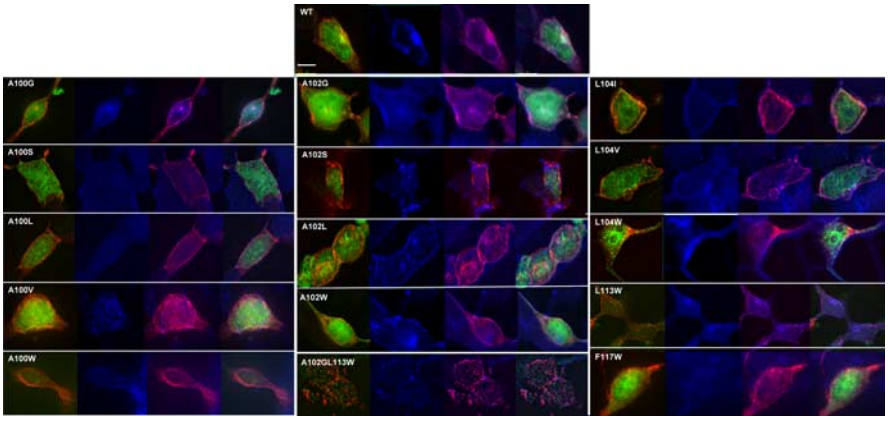

Figure 2. Membrane expression of prestin and mutants. ***A***, Wild-type prestin localizes to the cell membrane by 48 h after transfection. Prestin mutants are also expressed at the membrane by 48 h, and prestin fluorescence (red) coincides with that of WGA (blue), which stains GM1 gangliosides on the cell surface. In each case, the first panel shows prestin (red) and GFP (green) fluorescence, the second shows membrane (WGA) fluorescence (blue), the third panel is an overlay (pink) of prestin and WGA fluorescence, and the fourth is a merge of all panels. Scale bar, 10 μm.

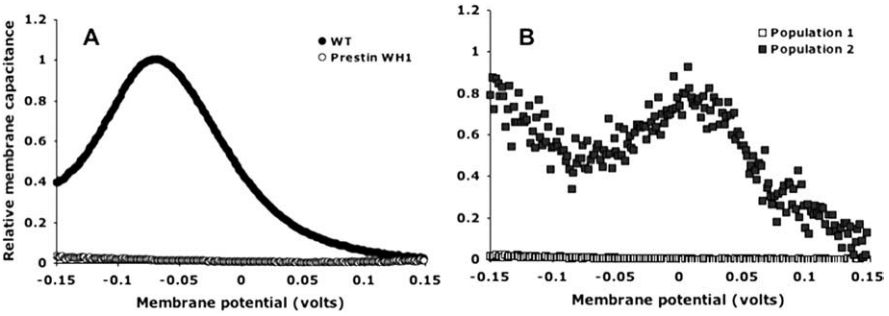

Figure 3. Normalized membrane capacitance of WT prestin, prestin^{WH1}, and prestin^{WH2}. ***A***, Normalized membrane capacitance of WT prestin (●), showing nonlinear (voltage dependent) capacitance. Also represented is a normalized membrane capacitance plot of prestin^{WH1} (○) (at bottom). ***B***, Normalized membrane capacitance plot from representative cells from prestin^{WH2} population 1, showing lack of NLC (□), and population 2, showing weak NLC (■). Raw data are presented in supplemental Figure 2 (available at www.jneurosci.org as supplemental material).

Prestin expression endows HEK 293 cells with NLC

All cells transfected with WT prestin (n = 31) exhibited NLC. A normalized (see equation above) bell-shaped NLC curve from a prestin-transfected HEK 293 cell is shown in Figure 3*A*. The signals obtained at both frequencies were very similar, with similar noise levels and a peak C at the same potential (supplemental Fig. 2, available at www.jneurosci.org as supplemental material). The main difference between them is C calculated at f is greater than at $2f$ for all potentials. When we examined the C versus V plots obtained from all cells, we found that voltage at peak capacitance V_{pkc} was -69.8 ± 18.1 mV and ranged from -95 to -39 mV. The average charge density was 11 ± 4 fC/pF. The capacitance–voltage function is qualitatively similar to that reported for cochlear OHCs, although the charge density is between 3 and 30% of that reported for OHCs [in which the charge density is 60–80 fC/pF (Santos-Sacchi, 1991]. The membrane resistance R_m was also dependent on the holding potential (supplemental Fig. 2, available at www.jneurosci.org as supplemental material), exhibiting a maximum ~0 V and decreasing monotonically on either side of the peak. This is also qualitatively similar to that observed with OHCs (Farrell et al., 2006), except R_m at and close to the peak is ~4 times greater in the prestin-transfected HEK 293 cells.

Prestin^{WH1} and prestin^{WH2} greatly reduce or eliminate NLC

We initially tested the NLC characteristics of prestin^{WH1} and prestin^{WH2}, which contained bulky W substitutions at A100/A102/L104 and L113/F117, respectively. All cells transfected with prestin^{WH1} (n = 11) showed no NLC. A typical normalized C versus V plot of prestin^{WH1} compared with WT is shown in Figure 3*A*. The plot does not exhibit the classic bell-shaped function indicative of prestin activity; the capacitance–voltage function is qualitatively similar to that observed for untransfected HEK 293 cells (Farrell et al., 2006). In most cells transfected with prestin^{WH2} (n = 17), the WT-like bell-shaped NLC was absent (Fig. 3*B*, open squares), but a proportion of cells (n = 8) exhibited a very small NLC with V_{pkc} at a more depolarized potential (Fig. 3*B*, filled squares).

Single amino acid substitutions in cluster 1 reveal size dependence

All single W substitutions in cluster 1 (A100W, A102W, and L104W) resulted in a capacitance profile similar to untransfected HEK 293 cells (Fig. 4*A–C*). However, for cluster 2, L113W exhibited a bell-shaped NLC curve similar to WT prestin but with a shift in the V_{pkc} to a more depolarized potential of 3.0 ± 11.6 mV (Fig. 5, Table 2). F117W showed NLC with a capacitance–voltage profile similar to WT (Fig. 5, Table 2).

We next made several single substitutions at each of the three trace residues in cluster 1, replacing A100 and A102 with G, L, V, and S and L104 with V and I. HEK 293 cells transfected with A100L, A100V, A102L, and A102V single mutants showed loss of NLC, with capacitance–voltage functions indistinguishable from that of untransfected HEK 293 cells (Fig. 4*A*,*B*). Importantly, cells transfected with A100G and A102G exhibited bell-shaped

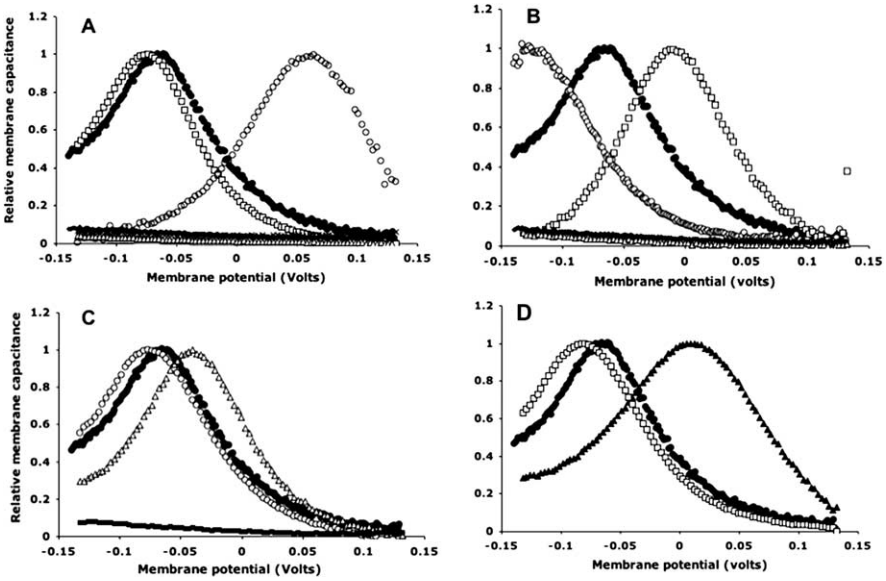

Figure 4. Normalized membrane capacitance of prestin single mutants. ***A***, Five single substitutions at A100: A100S (□), A102G (○), A102V (×), A102L (△), and A102W (□). A100V, L, and W (clustered at bottom) have minimal voltage dependence, similar to untransfected or mock-transfected controls. ***B***, Five single substitutions at A102: A102S (□), A102G (○), A102V (×), A102L (△), and A102W (□). A102V, L, and W have minimal voltage dependence, similar to untransfected or mock-transfected controls. ***C***, Three single substitutions at L104: L104V (□), L104I (△), and L104W (■). L104W has minimal voltage dependence, similar to untransfected or mock-transfected controls. ***D***, Capacitance plots of L113W (▲) and F117W (□). Representative plots, normalized relative to C (V_{pkc}) and C_{lin}, from single cells are shown (for absolute values of NLC magnitude; see Table 2). In all panels, a representative plot of WT prestin is shown for comparison (●). Differences in magnitude of NLC have been ignored in this representation (for details, see Table 2).

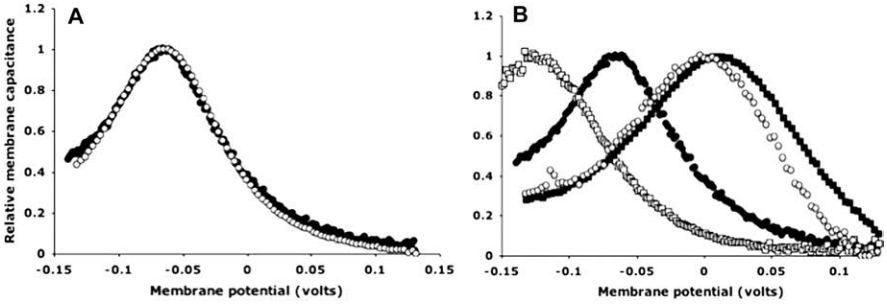

Figure 5. Normalized membrane capacitance of A305V and A102G/L113W. ***A***, Substitution of A305 with valine does not affect NLC. Cells transfected with A305V (○) exhibit a bell-shaped NLC curve indistinguishable from WT (●). ***B***, Cells transfected with A102G/L113W (○) exhibit a bell-shaped NLC curve with V_{pkc} between those of the two single mutants, A102G (□) and L113W (■). NLC of WT prestin is shown for comparison (●). Representative average traces from single cells are shown; for averages and deviations, see Table 2. Traces have been normalized relative to C (V_{pkc}) and C_{lin}. The average magnitude of NLC change was similar in A305V and WT (see Table 2).

capacitance curves similar to WT prestin but with V_{pkc} at more depolarized (A100G, 64.7 ± 13.8 mV) and more hyperpolarized (A102G, −124.2 ± 11.6 mV) voltages (Fig. 4*A*,*B*, Table 2). Cells transfected with A100S and L104V exhibited NLC traces indistinguishable from WT prestin (Fig. 4*A*,*C*, Table 2). Transfections with A102S and L104I produced bell-shaped NLC traces with V_{pkc} shifted slightly toward depolarized voltages (A102S, −7.3 ± 5.9 mV; L104I, 34.2 ± 3.2 mV) (Fig. 4*C*, Table 2).

The effects of substitutions at each trace residue in cluster 1 depend on the relative size of the original compared with the substituted residue. Replacement of the alanines at positions 100 and 102 with larger residues (V, L, and W) abolishes NLC, whereas substitution with the smaller residue G results in alterations in NLC. The substitution of S in place of A100 retains NLC characteristics similar to WT, consistent with the isostructural nature of S and A despite their chemical differences. However, the equivalent isostructural substitution at A102 results in altered V_{pkc}, indicating higher sensitivity to substitution at this position. In the case of L104, replacement with the similar branched-chain V does not affect NLC, whereas replacement with the straight-chain I shifts V_{pkc}. The cluster 2 trace residues, L113 and F117, do not follow this size-dependent trend, because replacement of L113 with W does not abolish NLC and replacement of F117 with the similar-sized W also results in WT-like NLC (Fig. 4*D*).

An alanine outside clusters 1 and 2 can be substituted without effect on NLC

To determine whether changes in NLC were restricted to substitutions at trace residues, we mutated A305, found at the helix–loop interface of helix 7 (Fig. 1), to V. This substitution with a larger residue had no effect on NLC and exhibited a bell-shaped capacitance curve similar to WT, with V_{pkc} at −58.5 ± 8.2 mV (Fig. 5*A*, Table 2).

Effect of the larger residue dominates in a double mutant

We generated a double mutant, A102G/L113W, substituting a smaller residue on helix 1 (cluster 1) and a larger residue on helix 2 (cluster 2). The corresponding single mutants, A102G and L113W, showed hyperpolarizing (V_{pkc} of −124.2 ± 11.6 mV) and depolarizing (V_{pkc} of +3.0 ± 11.6 mV) peak shifts, respectively. The double mutant exhibits a capacitance peak at −10.8 ± 19.2 mV, which is not statistically different from that of L113W (p = 0.18) (Fig. 5*B*). The charge density for this mutant, however, was significantly lower than WT prestin or the individual single mutants.

Discussion

SLC26A transporters are 11–13 transmembrane antiporters that promote the movement of anionic substrates (chloride, iodide, bicarbonate, and formate) with different specificities (Markovich, 2001; Vincourt et al., 2003; Mount and Romero, 2004). Mammalian prestins are unique because they have not been conclusively associated with conventional transport capabilities, although a recent model hypothesizes an antiport function (Muallem and Ashmore, 2006). The presence of ~12 TMs and the ability to couple anion exchange to the chemiosmotic gradient indicates common features between the human SLC26A family (transport classification number TC 2.A.53) and the major facilitator superfamily (MFS) (TC number 2.A.1; transporter classification database, http://www.tcdb.org). The transport mechanism of MFS members are postulated to involve alternating accessibility of a central substrate-binding site to either surface of the membrane

(Mitchell, 1957) caused by a conformational change in the transporter triggered by anion binding. A similar mechanism could explain conformational changes in prestin, triggered by cell potential changes.

Previous prestin functional mutation studies examined nonconserved charged residues (Oliver et al., 2001), glycosylation sites (Matsuda et al., 2004), phosphorylation sites (Deak et al., 2005), as well as domain swapping (Zheng et al., 2005) or C- and N-terminal deletions (Navaratnam et al., 2005; Zheng et al., 2005) and provided insights into prestin function by identifying residues or regions that affect prestin NLC. We used ET to identify critical functional residues in prestin and conducted a systematic mutational analysis, changing size, charge, or polarity of selected residues to better understand their contribution to prestin function.

ET analysis of prestin homologs revealed two highly ranked residue clusters in the region of the sulfate anion transporter motif (residues 109–130) (Mount and Romero, 2004), based on our predicted topology map of prestin (Fig. 1). Replacement of all residues in each cluster with tryptophan eliminated NLC (Fig. 3). Additional systematic replacements of cluster 1 residues (A100, A102, and L104) revealed size-dependent sensitivity to residue substitutions (Fig. 4*A–C*). Relatively normal NLC profiles were only seen when these residues were substituted with a smaller or isostructural amino acid. Cluster 2 residues (L113 and F117) did not appear to be dependent on residue size; replacement of L113 with W resulted in a bell-shaped, albeit peak-shifted NLC, whereas F117W closely resembled WT (Fig. 4*D*), but smaller substitutions may yield additional information on the role of this residue.

Interestingly, effects on NLC were observed only when residue size was changed, with hydrophobicity not a major contributing factor (except in the case of A102). In addition, these residues are not charged, leading to the assumption that they are not directly involved in charge movement. This is corroborated by the fact that certain substitutions at these residues retain NLC, albeit with altered peak characteristics. The identified residues, therefore, may be involved in helix packing, and perhaps in allosteric interactions, that influence conformational changes associated with charge movement.

A double mutant containing a smaller substitution (A102G) on helix 1 and a larger substitution (L113W) on helix 2 behaves similar to the L113W single mutant (Fig. 5*B*). A102 and L113 are adjacent to one another in helices 1 and 2, respectively; therefore, effects of a larger substitution at one of these residues might be compensated by a smaller substitution at the other. The V_{pkc} of the double mutant is slightly shifted toward the WT value (from the L113W value), but this is not statistically significant. The lack of compensation may be attributable to these two residues being not precisely in register or to the L113W substitution being too bulky for the smaller A102G substitution to compensate. This result, however, affirms that larger substitutions dominate the effect on prestin NLC, corroborating the theory of packing between residues.

All mutants that exhibited NLC showed charge densities comparable with WT, within SD limits (Fig. 6). The double mutant showed significantly lowered charge density, perhaps attributable to structural perturbation from multiple substitutions.

The A102S substitution showed a depolarizing shift in V_{pkc}, although the corresponding substitution at A100 showed WT-like NLC. Serine is more hydrophilic than alanine and might have the effect of perturbing protein–lipid interactions. Although A100 is tolerant of this change, the serine substitution at A102 on the opposite face of the helix does exhibit a significant effect on NLC. This might be an indication that the helical face containing A102 makes more contact with membrane components and/or with hydrophobic protein surfaces in the transmembrane region and therefore is less tolerant of a hydrophilic substitution.

An alanine outside the identified ET clusters was chosen to test the accuracy of ET predictions. A305 is located at the extracellular membrane interface of helix 7, at a similar position as A100, A102, and/or L104 in helix 1 of our topology map. Substitution of this residue with valine had no effect on the NLC profile (Fig. 5*A*), indicating that perturbation of helix packing in this region does not affect NLC.

We have therefore identified a region in prestin that is critical for normal prestin activity. This region, located near the sulfate anion transporter motif, appears to be tightly packed, intolerant of alterations in residue bulk, and may be involved directly or allosterically in conformational changes during prestin activity. It is worth mentioning that mutational studies on a plant sulfate transporter SHST1 indicate that tight packing of residues in helices 1 and 2 is necessary for sulfate transport by this protein (Shelden et al., 2001, 2003). It remains to be seen whether this region is directly involved in anion interactions that are essential for prestin activity (Oliver et al., 2001; Rybalchenko and Santos-Sacchi, 2003).

It has been proposed that intracellular chloride ions function as the voltage sensor of prestin, binding to a site in prestin, and translocating within the membrane in response to transmembrane voltage changes (Oliver et al., 2001). However, an anion-binding site on prestin, or any SLC26A transporter, has not been identified. Recent analyses of chloride-binding mechanisms of

Table 2. NLC characteristics (voltage at peak capacitance and charge density) of prestin mutants

Prestin mutant	Average voltage at peak capacitance (V_{pkc}) ± SD (mV)	Average charge density (fC/pF)	Sample size (no. of cells)
WT	−69.8 ± 18.1	11 ± 4	31
Prestin^{WH1}	NA	NA	11
Prestin^{WH2}	NA	NA	17
Prestin^{WH2}	24.2 ± 48.0	ND	8
A100S	−72.3 ± 7.7	10.7 ± 3.3	8
A100G	64.7 ± 13.8	6.4 ± 2.3	8
A100V	NA	NA	8
A100L	NA	NA	7
A100W	NA	NA	6
A102S	−7.3 ± 5.9	7.5 ± 3.7	8
A102G	−124.2 ± 11.6	10.4 ± 3.0	10
A102L	NA	NA	6
A102V	NA	NA	8
A102W	NA	NA	6
L104V	−78.8 ± 7.9	5.8 ± 3.5	7
L104I	34.2 ± 3.2	5.1 ± 2.8	7
L104W	NA	NA	6
L113W	3.0 ± 11.6	3.9 ± 2.8	8
F117W	−78.0 ± 10.6	11.6 ± 1.9	6
A305V	−58.5 ± 8.2	11.6 ± 5.1	7
A102G/L113W	−10.85 ± 19.2	4.0 ± 3.7	8

NA, Not applicable; ND, not determined.

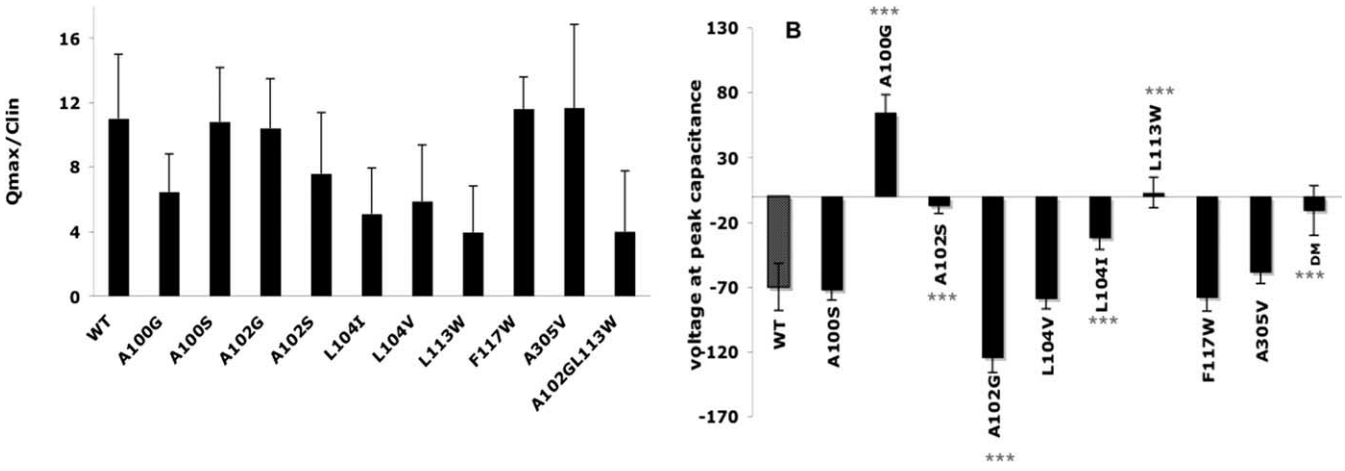

Figure 6. NLC characteristics of prestin and mutants. Average charge density (***A***) and average voltage at peak capacitance V_{pkc} (***B***) of single mutants are compared with wild type. Mutants A100V, A100L, A100W, A102V, A102L, A102W, and L104W are not represented in ***B*** because they did not exhibit bell-shaped capacitance curves. Unpaired *t* test was performed to evaluate statistical significance (**$p > 0.05$; ***$p > 0.0001$). In each case, this represents statistical significance of the mutant compared with WT values.

transporters and channels indicate that chloride is coordinated chiefly by partial positive charges from main-chain amides in these proteins (Dutzler et al., 2002; MacKinnon, 2004), with selectivity conferred by the size of the filter and not charge. By these criteria, helices 1 and 2 of prestin do indeed appear to be equipped to form a chloride-binding pocket; additional mutational studies are necessary for more detailed analysis.

Whether or not helices 1 and 2 line the actual chloride-binding pocket of prestin, it is clear that perturbations in the packing of these helices affect activity. In fact, the data can be correlated in broad mechanistic terms with the predicted topology map of prestin. A100 and A102 are two residues apart and therefore would be positioned on opposing surfaces of helix 1. Therefore, replacing A100 with a smaller side chain would have an opposite effect from a similar replacement at A102, in terms of helix packing. Although the direct effect on helix packing is unknown, the effect is very noticeable in terms of nonlinear capacitance. Replacement of A100 and A102 with the smaller glycine side chain shifts V_{pkc} of prestin NLC in opposite directions, suggesting that the packing of helix 1 against its adjacent helices is altered in opposing ways, which can be quantitatively correlated to changes in NLC characteristics. Furthermore, if helices 1 and 2 pack against each other, based on our two-dimensional topology, then replacement of L113 with W would have the effect of moving these helices apart by introducing steric bulk between them, whereas replacement of A100 with G would create more freedom for helix 1, allowing it to pack less closely with helix 2. In other words, L113W and A100G would produce similar effects, and, in fact, the data show that the effect of both these mutants is a positive shift of V_{pkc}, albeit to different extents. In addition, the A102G/L113W double mutant is not statistically distinguishable from L113W, indicating the dominance of a larger over a smaller substitution, as expected if the residues are closely packed.

A variety of manipulations that result in V_{pkc} changes include changes in membrane properties induced mechanically (Kakehata and Santos-Sacchi, 1995; Santos-Sacchi et al., 2001; Dong and Iwasa, 2004), chemically (Santos-Sacchi, 1991; Shehata et al., 1991; Tunstall et al., 1995; Kakehata and Santos-Sacchi, 1996; Lue et al., 2001), by temperature (Meltzer and Santos-Sacchi, 2001), or mutations (Oliver et al., 2001; Matsuda et al., 2004; Deak et al., 2005; Navaratnam et al., 2005; Zheng et al., 2005). Electromotility in OHCs represents a strong, reciprocal coupling of electrical and mechanical energy; therefore, changes in stress/polarization of the membrane result in peak shifts. We suggest that point mutations in the sulfate transporter motif alter the integrity of the membrane domains around prestin such that changes in both the electrical field in the membrane or membrane tension result in the observed peak shifts.

In summary, we used ET analysis to identify candidate functionally important residues in prestin. We generated systematic mutations at each residue, varying hydrophobicity, polarity, and size. The results indicate a possible functional role for the region of the conserved SLC26A sulfate anion transporter motif in prestin activity. Mutations of the corresponding residues in prestin orthologs such as pendrin would yield information of the functional significance, if any, of this region in transport processes of other SLC26A family proteins. In addition, substitutions of these amino acids in other SLC26A proteins might be used to confer prestin-like activity to these proteins.

References

Brownell WE (2006) The piezoelectric outer hair cell. In: Vertebrate hair cells (Eatock RA, ed), pp 313–347. New York: Springer.

Brownell WE, Bader CR, Bertrand D, de Ribaupierre Y (1985) Evoked mechanical responses of isolated cochlear outer hair cells. Science 227:194–196.

Brownell WE, Spector AA, Raphael RM, Popel AS (2001) Micro- and nanomechanics of the cochlear outer hair cell. Annu Rev Biomed Eng 3:169–194.

Dallos P, Fakler B (2002) Prestin, a new type of motor protein. Nat Rev Mol Cell Biol 3:104–111.

Deak L, Zheng J, Orem A, Du G-G, Aguinaga S, Matsuda K, Dallos P (2005) Effects of cyclic nucleotides on the function of prestin. J Physiol (Lond) 563:483–496.

Dong X-X, Iwasa KH (2004) Tension sensitivity of Prestin: comparison with the membrane motor in outer hair cells. Biophys J 86:1201–1208.

Dutzler R, Campbell EB, Cadene M, Chait BT, MacKinnon R (2002) X-ray structure of a ClC chloride channel at 3.0 A reveals the molecular basis of anion selectivity. Nature 415:287–294.

Fakler B, Oliver D (2002) Functional properties of prestin—how the motormolecule works work. In: Biophysics of the cochlea: from molecule to model. Singapore: World Scientific.

Farrell B, Shope CD, Brownell WE (2006) Voltage dependent capacitance of human embryonic kidney (HEK) cells. Phys Rev E Stat Nonlin Soft Matter Phys 73:041930.

Frank G, Hemmert W, Gummer AW (1999) Limiting dynamics of high-frequency electromechanical transduction of outer hair cells. Proc Natl Acad Sci USA 96:4420–4425.

Geva A, Lassere TB, Lichtarge O, Pollitt SK, Baranski TJ (2000) Genetic mapping of the human C5a receptor. Identification Of transmembrane amino acids critical for receptor function. J Biol Chem 275:35393–35401.

Kakehata S, Santos-Sacchi J (1995) Membrane tension directly shifts voltage dependence of outer hair cell motility and associated gating charge. Biophys J 68:2190–2197.

Kakehata S, Santos-Sacchi J (1996) Effects of salicylate and lanthanides on outer hair cell motility and associated gating charge. J Neurosci 16:4881–4889.

Konvicka K, Campagne F, Weinstein H (2000) Iterative construction of residue-based diagrams of proteins: the RbDe web service. Protein Eng 13:395–396.

Liberman MC, Gao J, He DZ, Wu X, Jia S, Zuo J (2002) Prestin is required for electromotility of the outer hair cell and for the cochlear amplifier. Nature 419:300–304.

Lichtarge O, Bourne HR, Cohen FE (1996) An evolutionary trace method defines binding surfaces common to protein families. J Mol Biol 257:342–358.

Lichtarge O, Yamamoto KR, Cohen FE (1997) Identification of functional surfaces of the zinc binding domains of intracellular receptors. J Mol Biol 274:325–327.

Ludwig J, Oliver D, Frank G, Klocker N, Gummer AW, Fakler B (2001) Reciprocal electromechanical properties of rat prestin: the motor molecule from rat outer hair cells. Proc Natl Acad Sci USA 98:4178–4183.

Lue AJ-C, Zhao H-B, Brownell WE (2001) Chlorpromazine alters outer hair cell electromotility. Otolaryngol Head Neck Surg 125:71–76.

MacKinnon R (2004) Potassium channels and the atomic basis of selective ion conduction. Biosci Rep 24:75–100.

Madabushi S, Yao H, Marsh M, Kristensen DM, Philippi A, Sowa ME, Lichtarge O (2002) Structural clusters of evolutionary trace residues are statistically significant and common in proteins. J Mol Biol 8:139–154.

Madabushi S, Gross AK, Philippi A, Meng EC, Wensel TG, Lichtarge O (2004) Evolutionary trace of G protein-coupled receptors reveals clusters of residues that determine global and class-specific functions. J Biol Chem 279:8126–8132.

Markovich D (2001) Physiological roles and regulation of mammalian sulfate transporters. Physiol Rev 81:1499–1533.

Matsuda K, Zheng J, Du G-G, Klocker N, Madison LD, Dallos P (2004) N-linked glycosylation sites of the motor protein prestin: effects on membrane targeting and electrophysiological function. J Neurochem 89:928–938.

Meltzer J, Santos-Sacchi J (2001) Temperature dependence of non-linear capacitance in human embryonic kidney cells transfected with prestin, the outer hair cell motor protein. Neurosci Lett 313:141–144.

Mitchell P (1957) A general theory of membrane transport from studies of bacteria. Nature 180:134–136.

Monsigny M, Roche A-C, Sene C, Maget-Dana R, Delmotte F (1980) Sugar-lectin interactions: how does wheat-germ agglutinin bind sialoglycoconjugates? Eur J Biochem 104:147–153.

Mount DB, Romero MF (2004) The SLC26 gene family of multifunctional anion exchangers. Pflügers Arch 447:710–721.

Muallem DR, Ashmore JF (2006) An anion antiporter model of prestin, the outer hair cell motor protein. Biophys J 90:4035–4045.

Navaratnam D, Bai J-P, Samaranayake H, Santos-Sacchi J (2005) N-Terminal-mediated homomultimerization of prestin, the outer hair cell motor protein. Biophys J 89:3345–3352.

Oliver D, Fakler B (1999) Expression density and functional characteristics of the outer hair cell motor protein are regulated during postnatal development in rat. J Physiol (Lond) 519:791–800.

Oliver D, He DZ, Klocker N, Ludwig J, Schulte U, Waldegger S, Ruppersberg JP, Dallos P, Fakler B (2001) Intracellular anions as the voltage sensor of prestin, the outer hair cell motor protein. Science 292:2340–2343.

Rybalchenko V, Santos-Sacchi J (2003) Cl^- flux through a non-selective, stretch-sensitive conductance influences the outer hair cell motor of the guinea-pig. J Physiol (Lond) 547:873–891.

Santos-Sacchi J (1991) Reversible inhibition of voltage-dependent outer hair cell motility and capacitance. J Neurosci 11:3096–3110.

Santos-Sacchi J, Kakehata S, Takahashi S (1998) Effects of membrane potential on the voltage dependence of motility-related charge in outer hair cells of the guinea-pig. J Physiol (Lond) 510:225–235.

Santos-Sacchi J, Shen W, Zheng J, Dallos P (2001) Effects of membrane potential and tension on prestin, the outer hair cell lateral membrane motor protein. J Physiol (Lond) 531:661–666.

Shehata WE, Brownell WE, Dieler R (1991) Effects of salicylate on shape, electromotility and membrane characteristics of isolated outer hair cells from guinea pig cochlea. Acta Otolaryngol 111:707–718.

Shelden MC, Loughlin P, Tierney ML, Howitt S (2001) Proline residues in two tightly coupled helices of the sulfate transporter, SHST1 are important for sulfate transport. Biochem J 356:589–594.

Shelden MC, Loughlin P, Tierney ML, Howitt S (2003) Interactions between charged amino acid residues within transmembrane helices in the sulfate transporter SHST1. Biochemistry 42:12941–12949.

Snyder KV, Sachs F, Brownell WE (2003) The outer hair cell: a mechano-electrical and electromechanical sensor/actuator. In: Sensors and sensing in biology and engineering (Barth FG, Humphrey JAC, Secomb TW, eds), pp 71–95. Vienna: Springer.

Song L, Seeger A, Santos-Sacchi J (2005) On membrane motor activity and chloride flux in the outer hair cell: lessons learned from the environmental toxin tributyltin. Biophys J 88:2350–2362.

Sowa ME, He W, Wensel TG, Lichtarge O (2000) A regulator of G protein signaling interaction surface linked to effector specificity. Proc Natl Acad Sci USA 97:1483–1488.

Sowa ME, He W, Slep KC, Kercher MA, Lichtarge O, Wensel TG (2001) Prediction and confirmation of a site critical for effector regulation of RGS domain activity. Nat Struct Biol 8:234–237.

Tunstall MJ, Gale JE, Ashmore JF (1995) Action of salicylate on membrane capacitance of outer hair cells from the guinea-pig cochlea. J Physiol (Lond) 485:739–752.

Vincourt JB, Jullien D, Amalric F, Girard JP (2003) Molecular and functional characterization of SLC26A11, a sodium-independent sulfate transporter from high endothelial venules. FASEB J 17:890–892.

Zheng J, Shen W, He DZ, Long KB, Madison LD, Dallos P (2000) Prestin is the motor protein of cochlear outer hair cells. Nature 405:149–155.

Zheng J, Long KB, Shen W, Madison LD, Dallos P (2001) Prestin topology: localization of protein epitopes in relation to the plasma membrane. NeuroReport 12:1929–1935.

Zheng J, Du G-G, Matsuda K, Orem A, Aguiñaga S, Deák L, Navarrete E, Madison LD, Dallos P (2005) The C-terminus of prestin influences nonlinear capacitance and plasma membrane targeting. J Cell Sci 118:2987–2996.